Spatial distribution of photoelectrons participating in formation of x-ray absorption spectra

O. Šipr
Institute of Physics, Academy of Sciences of the Czech Republic, Cukrovarnická 10, 162 53 Praha 6, Czech Republic
(Received 7 January 2002; published 15 May 2002)

Interpretation of x-ray absorption near-edge structure (XANES) experiments is often done via analyzing the role of particular atoms in the formation of specific peaks in the calculated spectrum. Typically, this is achieved by calculating the spectrum for a series of trial structures where various atoms are moved and/or removed. A more quantitative approach is presented here, based on comparing the probabilities that a XANES photoelectron of a given energy can be found near particular atoms. Such a photoelectron probability density can be consistently defined as a sum over squares of wave functions which describe participating photoelectron diffraction processes, weighted by their normalized cross sections. A fine structure in the energy dependence of these probabilities can be extracted and compared to XANES spectrum. As an illustration of this technique, we analyze the photoelectron probability density at the Ti *K* pre-edge of TiS_2 and at the Ti *K*-edge of rutile TiO_2.

DOI: 10.1103/PhysRevB.65.205115 PACS number(s): 78.70.Dm

I. INTRODUCTION

X-ray absorption fine structure (XAFS) is being used for studying both the electronic and the real structure of solids. For high photoelectron energies ($E \gtrsim 200$ eV), the extended x-ray absorption fine structure (EXAFS) can be intuitively described in terms of backscattering of the excited photoelectron by neighboring atoms and the EXAFS analysis has become a standard tool for real structure investigations. On the other hand, x-ray absorption near-edge structure (XANES) is lagging behind in its applications for structural studies, despite some promising applications in selected systems.[1–4] The reason for this rests in a more complex physics hidden behind XANES, resulting both in a more difficult theoretical treatment (multiple scattering, self-consistency in potentials, non-muffin-tin effects) and in a lack of a proper intuitive insight into the formation of XANES peaks. The need for involving XANES in structural analysis stems partly from the fact that EXAFS is predominantly sensitive only to atomic distances and not to bond angles and partly from the high signal-to-noise ratio for some interesting classes of systems which severely limits the ability to extract EXAFS oscillations from their spectra.

A means to interpret XANES in intuitively plausible terms would, among others, facilitate application of XANES spectroscopy in investigations of both the real and the electronic structure. Various procedures were applied in the past with the aim to connect XANES spectral features with real structure. Among them, let us mention inspecting the effect of adding or removing certain atoms in the test cluster,[5] investigating the dependence of the height of the pre-peak on the geometry of the nearest neighborhood,[6] calculating XANES by summing over many scattering paths[7] or employing the ''direct inversion'' technique for obtaining the atomic positions and scattering potential from experimental XANES.[8] In this study, we would like to tackle the problem of interpreting XANES spectra from yet another side; namely, we want to explore the probability density of the photoelectrons. Such a procedure can be—from a certain viewpoint—considered as an answer to the naive question as to where the XANES photoelectron really is. Answering such a fundamental question would have implications for real structure as well as for electronic structure studies.

At the beginning of this paper, a general consideration of the problem will be outlined, the main goal being to define the task in exact terms. Then we will present few mathematical formulas which describe the problem and determine how the proper probability density ought to be evaluated. Next follows a discussion of some practical aspects of evaluating the photoelectron probability density and the technique is illustrated on the pre-edge structure of Ti *K*-edge of TiS_2 and on the whole Ti *K*-edge XANES of TiO_2. Some more technical details are given in the Appendixes.

II. LOCALIZATION OF THE PHOTOELECTRON

XAFS arises due to the energy dependence of the core-electron photoeffect: An electron absorbs an x-ray photon, is ejected off the atom, and starts to travel inside the solid. In a stationary picture, the wave function of the excited photoelectron can be viewed as being subject to multiple scattering by neighboring atoms. The probability of photoabsorption oscillates with energy—one can, especially in the EXAFS regime, interpret this oscillatory behavior intuitively as a consequence of either constructive or destructive interference of the photoelectron wave function. One can thus associate a particular spectral peak with scattering of a photoelectron of a certain energy. The topic of this section (and of this paper as a whole) is to explore the spatial localization of this photoelectron.

A. Wave function problem

In the framework of the quantum theory, the popular question as to where the electron is cannot be answered. However, it is possible to ask what is the probability density $P(\boldsymbol{r})$ that a quantum-mechanical object can be found at a given place $\boldsymbol{r}$—it is just the square of the modulus of its wave function,

$$P(\boldsymbol{r}) = |\psi(\boldsymbol{r})|^2. \tag{1}$$

So the problem is reduced to the task of finding the wave function $\psi_{\rm phe}(\boldsymbol{r})$ which would appropriately describe the photoelectron participating in the formation of XANES at a given energy.

The correct form of this wave function ought to emerge from the way of calculating the x-ray absorption spectrum. The x-ray absorption spectrum (XAS) intensity is proportional to the probability w that a photon is absorbed by a core electron. That can be expressed, within first-order perturbation theory, as

$$w = 2\pi \int d\nu |\langle \psi_\nu | H_I | \phi_c \rangle|^2 \delta(E_c + \omega - E_\nu), \qquad (2)$$

where H_I is the interaction Hamiltonian perturbing the initial electron state $|\phi_c\rangle$ and the sum or integration over ν spans *any* complete set of electron wave functions $|\psi_\nu\rangle$ (Rydberg atomic units are used throughout this paper, taking $m=1/2$, $\hbar=1$, $e^2=2$, $c=2/\alpha$, and $\alpha=1/137.036$). Applying standard procedures, Eq. (2) can be transformed into expressions which involve either sums over Bloch states[9] or molecular cluster basis functions[10] or photoelectron diffraction states,[11] or which, in the case of Green function formalism, dispose of the final-state wave functions altogether.[12] The important factor is that the choice of the set of wave functions $|\psi_\nu\rangle$ does not affect the outcome of Eq. (2). This is favorable, on the one hand, as one does not have to care about the particular form of wave functions $|\psi_\nu\rangle$ when calculating XAS intensity. On the other hand, it means that the proper photoelectron wave function cannot just be borrowed from Eq. (2) or from any of its clones.

A close look at Eq. (2) reveals that the situation is even worse at the first sight. Namely, it follows from Eq. (2) that the total absorption rate is actually resultant from many *incoherent* processes. Hence, there is simply *no single wave function* like $|\psi_{\rm phe}\rangle$ which could have been inserted into Eq. (1). Nevertheless, one still can ask what the probability is that any electron ejected as a result of the absorption of a photon with energy ω can be found at $\boldsymbol{r}$. One only has to reformulate the problem slightly: Instead of searching for $|\psi_{\rm phe}(\boldsymbol{r})|^2$, the quantity of interest should rather be a weighted sum of probability densities of those wave functions which describe states participating in the absorption process,[13]

$$P(\boldsymbol{r}) = \sum_f w_f |\psi_f(\boldsymbol{r})|^2. \qquad (3)$$

The weights w_f with which the participating wave functions contribute to $P(\boldsymbol{r})$are the probabilities that a core electron $|\phi_c\rangle$ is ejected into the state $|\psi_f\rangle$,

$$w_f \sim |\langle \phi_c | H_I | \psi_f \rangle|^2. \qquad (4)$$

They ought to be normalized so that their sum yields the total XAS probability w. Note that all this is just another way of saying that the ejected photoelectron is described not by a single quantum state but rather by a density matrix,

$$V = \sum_f w_f |\psi_f\rangle\langle\psi_f|. \qquad (5)$$

Unfortunately, there appears to be a complication resulting from the use of Eqs. (3) and (4). Unlike in the case of Eq. (2), the outcome of Eqs. (3) and (4) now, namely, *does depend* on the choice of the set of wave functions $|\psi_f\rangle$ [complete on the energy surface determined by the δ function in Eq. (2)]. There is no way to fix this choice by relying solely on Eq. (2). It is a matter of physical intuition, not formal mathematical procedures, to establish which set of states $|\psi_f\rangle$ is relevant to the physical process in question. A guide for this choice could be the conservation of electron number: As one has one electron in the initial state (it is the core electron $|\phi_c\rangle$), one has to end up with one electron in the final state as well.

The choice of states $|\psi_f\rangle$ is quite straightforward in the case of transitions to bound states (say, of a molecule). The final states $|\psi_f\rangle$ are just asymptotically decaying bound states $|\psi_b\rangle$, normalizable so that $\int d^3\boldsymbol{r} |\psi_b(\boldsymbol{r})|^2 = 1$. The situation is more complicated for transitions to the continuous part of the spectrum, as there is no *a priori* preference for normalization and/or boundary conditions which such a wave function ought to observe.

In order to find the correct wave functions, let us contemplate a finite cluster of atoms (a situation tacitly assumed in most applications of the real-space formalism) (Refs. 10–12) and follow the fate of the initially core electron. As a result of absorbing a photon, this electron is torn off an atom and, having its energy above the continuum threshold, must finally leave the cluster and turn into a plane wave with a well-defined momentum direction $\hat{\boldsymbol{k}}$. This means that the elementary incoherent processes involved in the sum (3) must be *photoelectron diffraction* events. Indeed, x-ray absorption is conceptually nothing else but angularly integrated photoelectron diffraction (PED).[11,14] The final states $|\psi_f\rangle$ are, therefore, time-inversed scattering states $|\psi_{\boldsymbol{k}}^{(-)}\rangle$, which are in turn solutions of the Lippman-Schwinger equation[11,15,16]

$$\psi_{\boldsymbol{k}}^{(-)}(\boldsymbol{r}) = e^{i\boldsymbol{k}\cdot\boldsymbol{r}} + \int d^3\boldsymbol{r}' G_0^{(-)}(\boldsymbol{r},\boldsymbol{r}') V(\boldsymbol{r}') \psi_{\boldsymbol{k}}^{(-)}(\boldsymbol{r}'), \qquad (6)$$

where $G_0^{(-)}(\boldsymbol{r},\boldsymbol{r}')$ is the advanced free electron Green function and $V(\boldsymbol{r}')$ describes the potential of the cluster. The states $|\psi_{\boldsymbol{k}}^{(-)}\rangle$ are normalizable to the delta function $\delta(\boldsymbol{k})$ [apart from the constant factor $1/(2\pi)^{3/2}$], which guarantees that they describe exactly one electron at a time.[15]

The probability density $P(\boldsymbol{r})$ obtained via Eqs. (3) and (4) cannot be normalized to 1. However, due to Eq. (6), it can be related to the probability density of a free electron, which is described by the wave function $\exp(i\boldsymbol{k}\cdot\boldsymbol{r})$ and holds thus a constant probability density everywhere. So the probability density $P(\boldsymbol{r})$ is actually measured in ''units of free-electron probability density.'' Thus, by pegging the normalization of $|\psi_f\rangle$ to the normalization of the free-electron wave function $\exp(i\boldsymbol{k}\cdot\boldsymbol{r})$, one keeps a universal definition of $P(\boldsymbol{r})$.

Intuitively, the wave function $|\psi_{\boldsymbol{k}}^{(-)}\rangle$ can be viewed as that wave function, from which a plane wave evolves within

a sufficiently long time. It represents the state into which the core electron ''jumps'' as a result of the electromagnetic perturbation H_I. Thus, the quantity $P(\boldsymbol{r})$ ought to be interpreted as the probability that the electron ejected from a core level can be found at position $\boldsymbol{r}$, ''just after'' having absorbed an x-ray photon. By evaluating $P(\boldsymbol{r})$, one provides the most sensible answer to the seemingly naive question about the localization of the XANES photoelectron. We bear in mind, at the same time, that this Lippman-Schwinger-like description cannot fully substitute for a proper time-dependent treatment.[17]

B. Evaluating the photoelectron probability density $P(\boldsymbol{r})$

In this section, we present equations necessary for calculating the photoelectron probability density $P(\boldsymbol{r})$. Although some of them can be found in that or other form in various papers dealing with x-ray absorption or photoelectron diffraction theory (especially in Refs. 16 and 18), we present them here anyway in order to embed them into the context of this work, to offer the reader a complete set of equations which might be helpful for practical calculations, and, last but not least, to unify various notation and conventions.

The proper mathematical expression for evaluating the probability density of electrons participating in x-ray absorption process can be obtained by inserting the wave function $|\psi_{\boldsymbol{k}}^{(-)}\rangle$ into Eqs. (3) and (4). We get

$$P(\boldsymbol{r})=\frac{1}{\sigma_{\mathrm{XAS}}}\int d^2\hat{\boldsymbol{k}}\,\frac{d\sigma}{d\Omega_{\boldsymbol{k}}}|\psi_{\boldsymbol{k}}^{(-)}(\boldsymbol{r})|^2, \tag{7}$$

where the PED cross section $d\sigma/d\Omega_{\boldsymbol{k}}$ stems from the partial probability w_f of Eq. (4) and the XAS cross section σ_{XAS},

$$\sigma_{\mathrm{XAS}}=\int d^2\hat{\boldsymbol{k}}\,\frac{d\sigma}{d\Omega_{\boldsymbol{k}}}, \tag{8}$$

ensures correct normalization.

By keeping only the dipole and quadrupole terms in the electromagnetic Hamiltonian H_I, the PED cross section can be written as

$$\frac{d\sigma}{d\Omega_{\boldsymbol{k}}}=\frac{1}{4\pi}\alpha\omega k[|\langle\psi_{\boldsymbol{k}}^{(-)}|\hat{\boldsymbol{\varepsilon}}\cdot\boldsymbol{r}|\phi_c\rangle|^2+|\langle\psi_{\boldsymbol{k}}^{(-)}|(\hat{\boldsymbol{\varepsilon}}\cdot\boldsymbol{r})\times(\hat{\boldsymbol{q}}\cdot\boldsymbol{r})|\phi_c\rangle|^2], \tag{9}$$

where $\boldsymbol{\varepsilon}$ is the polarization vector of the incoming radiation and $\boldsymbol{q}$ is its wave vector ($\boldsymbol{q}=1/2\,\alpha\omega\hat{\boldsymbol{q}}$). Employing the muffin-tin approximation, the wave functions $\psi_{\boldsymbol{k}}^{(-)}(\boldsymbol{r})$ can be expanded inside the jth muffin-tin sphere as

$$\psi_{\boldsymbol{k}}^{(-)}(\boldsymbol{r})=\sum_L \beta_L^{(j)}(\boldsymbol{k})\mathcal{R}_l^{(j)}(kr)Y_L(\hat{\boldsymbol{r}}), \tag{10}$$

where single-sphere solutions of the radial Schrödinger equation $\mathcal{R}_l^{(j)}(kr)$ are normalized so that they smoothly match the free-space solution

$$\mathcal{R}_l^{(j)}(kr)=\cot\delta_l^{(j)}j_l(kr)-n_l(kr) \tag{11}$$

outside the muffin-tin sphere. The double subscript L stands for the pair (l,m).

Following the formalism of Ref. 16, the coefficients $\beta_L^{(j)}(\boldsymbol{k})$ can be expanded as

$$\beta_L^{(j)}(\boldsymbol{k})=4\pi\sum_{L''} i^{l''}\beta_L^{(j)}(L'')Y_{L''}^*(\hat{\boldsymbol{k}}), \tag{12}$$

where the amplitudes $\beta_L^{(j)}(L'')$ satisfy

$$\beta_L^{(j)}(L'')=\sum_{pL'} W_{LL'}^{jp}J_{L'L''}^{p0}. \tag{13}$$

The scattering matrix W is an inverse matrix to

$$[W^{-1}]_{LL'}^{ij}=(\sin\delta_l^{(j)}e^{-i\delta_l^{(j)}})^{-1}\delta_{ij}\delta_{LL'}+4\pi(1-\delta_{ij})\times\sum_{L_1} i^{l-l'+l_1}ih_{l_1}^{(-)}(k|\boldsymbol{R}^{ij}|)Y_{L_1}(\hat{\boldsymbol{R}}^{ij})C_{LL_1}^{L'}, \tag{14}$$

where the Gaunt symbol $C_{LL_1}^{L'}$ stands for

$$C_{LL_1}^{L'}=\int d^2\hat{\boldsymbol{n}}Y_L(\hat{\boldsymbol{n}})Y_{L'}^*(\hat{\boldsymbol{n}})Y_{L_1}(\hat{\boldsymbol{n}}), \tag{15}$$

the free-electron propagator $J_{LL'}^{pq}$ is

$$J_{LL'}^{pq}=4\pi\sum_{L_1} i^{l-l'+l_1}j_{l_1}(k|\boldsymbol{R}^{pq}|)Y_{L_1}(\hat{\boldsymbol{R}}^{pq})C_{LL_1}^{L'}, \tag{16}$$

and $\boldsymbol{R}^{ij}$ is defined as

$$\boldsymbol{R}^{ij}=\boldsymbol{R}^i-\boldsymbol{R}^j. \tag{17}$$

The amplitudes $\beta_L^{(j)}(L'')$ and the scattering matrix $W_{LL'}^{ij}$ are ''incoming-wave'' analogs of the amplitudes $B_L^{(j)}(L'')$ and the scattering matrix $[(\underline{T}+\underline{H})^{-1}]_{LL'}^{ij}$, employed in Ref. 16 for analyzing the scattering of an electron by a molecule. See Appendix A for a more comprehensive comparison.

Employing the amplitudes $\beta_L^{(j)}(L'')$, the PED cross section can be expressed via

$$\frac{d\sigma}{d\Omega_{\boldsymbol{k}}}=4\pi\alpha\omega k\left\{\left|\sum_L\sum_{L''}(-i)^{l''}[\beta_L^{(0)}(L'')]^*Y_{L''}(\hat{\boldsymbol{k}})D_{LL_c}\right|^2+\frac{1}{16}\alpha^2\omega^2\left|\sum_L\sum_{L''}(-i)^{l''}[\beta_L^{(0)}(L'')]^*Y_{L''}(\hat{\boldsymbol{k}})Q_{LL_c}\right|^2\right\}, \tag{18}$$

where the dipole and quadrupole matrix elements are

$$D_{LL_c}\equiv\int drr^3\mathcal{R}_l^{(0)}(kr)\phi_c(r)\int d^2\hat{\boldsymbol{r}}\;Y_L^*(\hat{\boldsymbol{r}})\hat{\boldsymbol{\varepsilon}}\cdot\hat{\boldsymbol{r}}Y_{L_c}(\hat{\boldsymbol{r}}) \tag{19}$$

and

$$Q_{LL_c} \equiv \int dr r^4 \mathcal{R}_l^{(0)}(kr)\phi_c(r) \int d^2\hat{\boldsymbol{r}}\, Y_L^*(\hat{\boldsymbol{r}})(\hat{\boldsymbol{\varepsilon}}\cdot\hat{\boldsymbol{r}})(\hat{\boldsymbol{q}}\cdot\hat{\boldsymbol{r}})Y_{L_c}(\hat{\boldsymbol{r}}) \tag{20}$$

and L_c specifies the angular momentum of the core state located at the central atom $\boldsymbol{R}^0$.

The XAS cross section follows from Eq. (8) and Eq. (18) as

$$\sigma_{\mathrm{XAS}} = 4\pi\alpha\omega k \sum_{L''} \left\{ \left| \sum_L [\beta_L^{(0)}(L'')]^* D_{LL_c} \right|^2 + \frac{1}{16}\alpha^2\omega^2 \left| \sum_L [\beta_L^{(0)}(L'')]^* Q_{LL_c} \right|^2 \right\}, \tag{21}$$

resembling in this form analogous expressions presented, e.g., in Refs. 10 and 16 (note that we ignore the electron spin throughout this paper). Again, in Appendix A we will present few other equivalent formulations of Eqs. (18) and (21).

Considering Eqs. (7) and (10), one obtains the expression for probability density of ejected photoelectron inside the jth muffin-tin sphere as

$$P(\boldsymbol{r}) = \frac{1}{\sigma_{\mathrm{XAS}}} \int d^2\hat{\boldsymbol{k}} \frac{d\sigma}{d\Omega_{\boldsymbol{k}}} \left| \sum_L \beta_L^{(j)}(\boldsymbol{k})\mathcal{R}_l^{(j)}(kr)Y_L(\hat{\boldsymbol{r}}) \right|^2, \tag{22}$$

where the PED and XAS cross sections have to be taken from Eqs. (18) and (21).

In electronic structure studies, it might be helpful to have a tool for investigating the angular momentum character of photoelectrons with respect to a site $\boldsymbol{R}^j$. That can be achieved by inserting into the sum (3) only the angular-momentum projected parts of photoelectron wave functions,

$$P_l(\boldsymbol{r}) = \sum_f w_f |\mathsf{P}_l \psi_f(\boldsymbol{r})|^2, \tag{23}$$

where P_l stands for the relevant projection operator. Analogously to Eq. (22), one gets the probability density of finding a XANES photoelectron at position $\boldsymbol{r}$ with an angular momentum l with respect to the site $\boldsymbol{R}^j$ as

$$P_l(\boldsymbol{r}) = \frac{1}{\sigma_{\mathrm{XAS}}} \int d^2\hat{\boldsymbol{k}} \frac{d\sigma}{d\Omega_{\boldsymbol{k}}} \left| \sum_m \beta_{lm}^{(j)}(\boldsymbol{k})\mathcal{R}_l^{(j)}(kr)Y_{lm}(\hat{\boldsymbol{r}}) \right|^2, \tag{24}$$

meaning that the sum Σ_L in Eq. (22) was just substituted with Σ_m.

C. Practical aspects

This study is motivated by an effort to understand x-ray absorption spectra and, in particular, to develop a means of connecting spectral and structural features. It is thus desirable to explore how $P(\boldsymbol{r})$ depends on the energy of the photoelectron. A simple way to extract the fine structure from this dependence is to subtract from $P(\boldsymbol{r})$ the probability which would correspond to a single isolated atom—just like the EXAFS can be extracted from a raw absorption spectrum by subtracting from it the atomic part (sometimes called AXAFS or atomic XAFS).[19] The single-atom probability density $P_{\mathrm{ato}}(\boldsymbol{r})$ can be evaluated following the procedure outlined in Sec. II B, taking into account only a single scatterer (cf. Appendix B). By investigating the difference $P(\boldsymbol{r}) - P_{\mathrm{ato}}(\boldsymbol{r})$, one can see more clearly the effects of surrounding atoms on the formation of both XANES and the photoelectron probability density.

In practice, one often wants to compare the importance of particular atoms for generating XAFS. For that purpose, it is sufficient to compare not $P(\boldsymbol{r})$ but rather its integrals inside suitably chosen spheres. We can define atomic-site-related quantities $P^{(j)}$and $\Delta P_{\mathrm{ato}}^{(j)}$by

$$P^{(j)} \equiv \frac{1}{V^{(j)}} \int_0^{R_N^{(j)}} dr r^2 \int d^2\hat{\boldsymbol{r}}\, P(\boldsymbol{r}), \tag{25a}$$

$$\Delta P_{\mathrm{ato}}^{(j)} \equiv \frac{1}{V^{(j)}} \int_0^{R_N^{(j)}} dr r^2 \int d^2\hat{\boldsymbol{r}} [P(\boldsymbol{r}) - P_{\mathrm{ato}}(\boldsymbol{r})] \tag{25b}$$

where $R_N^{(j)}$ is a suitably chosen normalization radius and $V^{(j)}$ is the volume of the normalization sphere around the jth site. Note that in the case of muffin-tin approximation, only spherically averaged values make sense anyway.

From the XANES analysis point of view, the quantities $P^{(j)}$, $\Delta P_{\mathrm{ato}}^{(j)}$ contain still quite a lot of unnecessary or "ballast" information. This is due to the fact that the probability density $P(\boldsymbol{r})$ defined by Eq. (7) is dominated by isotropic density of states (DOS) effects, which are *not specific to the site from which the photoelectron is ejected*.[20] This DOS-like contribution can be quantified by defining a DOS-like probability density $P_{\mathrm{DOS}}(\boldsymbol{r})$, which differs from $P(\boldsymbol{r})$by assuming a $\hat{\boldsymbol{k}}$-independent or "unidirectional" photoelectron diffraction cross section $d\sigma/d\Omega$ as[13]

$$P_{\mathrm{DOS}}(\boldsymbol{r}) \equiv \frac{1}{\sigma_{\mathrm{XAS}}} \frac{d\sigma}{d\Omega} \int d^2\hat{\boldsymbol{k}} |\psi_{\boldsymbol{k}}^{(-)}(\boldsymbol{r})|^2 = \frac{1}{4\pi} \int d^2\hat{\boldsymbol{k}} |\psi_{\boldsymbol{k}}^{(-)}(\boldsymbol{r})|^2. \tag{26}$$

Thus states with different $\hat{\boldsymbol{k}}$ contribute to $P_{\mathrm{DOS}}(\boldsymbol{r})$ with identical weights, just as is the case of local $\boldsymbol{r}$-dependent DOS. It can be shown easily that $P_{\mathrm{DOS}}(\boldsymbol{r})$ is indeed proportional to the density of states $n(\boldsymbol{r},E)$,

$$n(\boldsymbol{r},E) = -\frac{1}{\pi} \mathrm{Im}\, G^{(+)}(\boldsymbol{r},\boldsymbol{r};E) = \frac{k}{4\pi^2} P_{\mathrm{DOS}}(\boldsymbol{r}). \tag{27}$$

An atomic-sphere-related quantity $\Delta P_{\mathrm{DOS}}^{(j)}$ can be defined analogously to Eq. (25),

$$\Delta P_{\mathrm{DOS}}^{(j)} \equiv \frac{1}{V^{(j)}} \int_0^{R_N^{(j)}} dr r^2 \int d^2\hat{\boldsymbol{r}} [P(\boldsymbol{r}) - P_{\mathrm{DOS}}(\boldsymbol{r})]. \tag{28}$$

Typically, P does not differ from P_{DOS} by more than 10% (but often much less). Specific XAS-related effects may thus be obscured in $P(\boldsymbol{r})$ by more general DOS effects. The difference probability density $P(\boldsymbol{r}) - P_{\mathrm{DOS}}(\boldsymbol{r})$ informs how the spatial localization of a XANES electron differs from the spatial localization of a "generic" electron (with the same

energy). By investigating the difference probability $\Delta P^{(j)}_{\mathrm{DOS}}$, one can filter out effects which are not specific for XAS.

Generally, the total probability density $P^{(j)}$ informs where the most of the photoelectron is located, while the difference probability density $\Delta P^{(j)}_{\mathrm{DOS}}$ is especially sensitive to the photon polarization $\boldsymbol{\varepsilon}$ and to the position of the photoabsorbing atom. We postpone a further discussion of these concepts to Sec. III A, where they will be illustrated on a concrete example.

III. APPLICATION OF PHOTOELECTRON PROBABILITY DENSITY ANALYSIS

We explore the potential of photoelectron probability density (PEPD) analysis by examining several XANES spectra, which were subdued to investigation of the origin of their peaks in the past. In particular, we will concentrate on the pre-peak at the Ti *K*-edge XANES of TiS_2 and on the whole Ti *K*-edge XANES of rutile TiO_2.

All the calculations presented here were done for a non-self-consistent muffin-tin potential constructed via Mattheiss prescription (superposition of charge densities of isolated atoms). Using non-self-consistent potentials is not a serious drawback in this case as our aim is not to achieve the best reproduction of experimental spectra but to demonstrate a method how the calculated spectra can be analyzed.

The exchange-correlation potential of Ceperley and Adler[21] was used for atomic calculations of occupied states. In constructing the Mattheiss potential appropriate for unoccupied states, an energy-independent $X\alpha$ potential with the Kohn-Sham value of $\alpha=0.66$ was used.[22] Structural data were taken from the CRYSTIN database.[23] Only dipole transitions were taken into account. This limitation is justified in this study because it was demonstrated experimentally that quadrupole transitions do not contribute to the TiS_2 pre-peak intensity significantly[24] and in the case of TiO_2 spectrum our concern is with the main peaks and the extended XANES region, where the quadrupole contribution again is negligible. Muffin-tin radii of nonoverlapping spheres were determined so that single-site potentials, which were being superimposed, matched at the touching points (''matching potential condition''). The muffin-tin zero was set to the average interstitial potential. The influence of the core hole left on the central atom by the excited electron was taken into account by calculating the central atom charge density with one electron being moved from the $1s$ core level to the lowest unoccupied atomic orbital (a relaxed and screen model). A more thorough discussion of how the potential is constructed can be found, e.g., in Refs. 5 and 25.

When evaluating the sphere-averaged quantities $P^{(j)}$, $\Delta P^{(j)}_{\mathrm{ato}}$, and $\Delta P^{(j)}_{\mathrm{DOS}}$ according to Eqs. (25) and (28), one has to choose the normalization radius $R_N^{(j)}$ for each of the spheres. Throughout this section, we always take $R_N^{(j)}$ identical for all atoms of a given compound and equate it with the smallest of muffin-tin radii. We found that changing $R_N^{(j)}$ affects rather the overall magnitude of PEPD than its fine structure. Consequently, the overall picture, as presented in Secs. III A–III B, does not depend on the choice of $R_N^{(j)}$.

Experimental x-ray absorption spectra are broadened with respect to ''raw'' theoretical spectra because of various many-body processes (finite core hole lifetime, extrinsic photoelectron losses, etc.). It is thus desirable to anticipate this smearing when evaluating the PEPD's — otherwise, one would be overburdened with too many details with little or no physical significance. Therefore, we modified the scattering potential by adding to it a small negative imaginary part. We set its magnitude so that it simulates Lorentzian broadening equivalent to the half of a natural core hole width (taken from compilation of Al Shamma *et al.*)[26] Such a procedure would certainly be insufficient if one tried to describe the spectral broadening in a realistic way — apart from too small core hole smearing, energy-dependent inelastic energy losses of the photoelectron are unaccounted for altogether. However, as our main aim is to analyze the peaks in the *calculated* spectrum, we prefer to include less damping in order to have certain features more pronounced. We checked that increasing the imaginary potential twice would not affect the outcome of our analysis considerably.

A. Pre-peak at Ti *K*-edge of TiS_2

TiS_2 has a layered crystal structure consisting of sulphur-titanium-sulphur slabs. Each of these slabs is formed by a two-dimensional hexagonal titanium sublattice sandwiched by two closely adjacent sulphur hexagonal sublattices. Locally, the titanium atom is octahedrally coordinated by six sulphur atoms (cf. Fig. 3 of Ref. 27); the second coordination shell is formed by Ti atoms of the same hexagonal sublattice to which the central Ti atom belongs.

The polarized Ti *K*-edge XANES of TiS_2 shows a distinct pre-peak at the xy polarization (i.e., when the polarization vector of the incoming radiation lies within the titanium layer).[27,28] Relying on XANES calculations for artificial trial structures, Wu *et al.*[27] suggested that the pre-edge is generated by multiple scattering which involves mainly the central Ti atom and the Ti atoms of the second coordination shell.

A comprehensive analysis of the Ti *K*-edge XANES of TiS_2, including comparison between theory and experiment, can be found elsewhere.[27,28,24] Therefore, we present in Fig. 1 only the theoretical polarized pre-peak structure, calculated for a cluster of 135 atoms, together with $P^{(j)}$, $\Delta P^{(j)}_{\mathrm{ato}}$, and $\Delta P^{(j)}_{\mathrm{DOS}}$ curves for the central atom and for atoms of its four nearest coordination shells. Two polarizations correspond to the $\boldsymbol{\varepsilon}$ vector averaged over the full 2π angle within the xy plane and to the $\boldsymbol{\varepsilon}\|z$ setup. Titanium probability densities are scaled down by a factor of 20 with respect to corresponding sulphur curves, as indicated. Individual atoms belonging to the same coordination shell give rise to identical PEPD's in this case (also for further shells than those displayed in Fig. 1). As we did not perform a band-structure calculation, the Fermi level is not fixed. It follows from Fig. 1 that it ought to be around $\approx$6 eV above the muffin-tin zero; therefore, all states below it are actually occupied and do not contribute to the x-ray absorption spectrum—we show them just for completeness.

The first information one gets from Fig. 1 is that the photoelectron probability density clearly oscillates with energy.

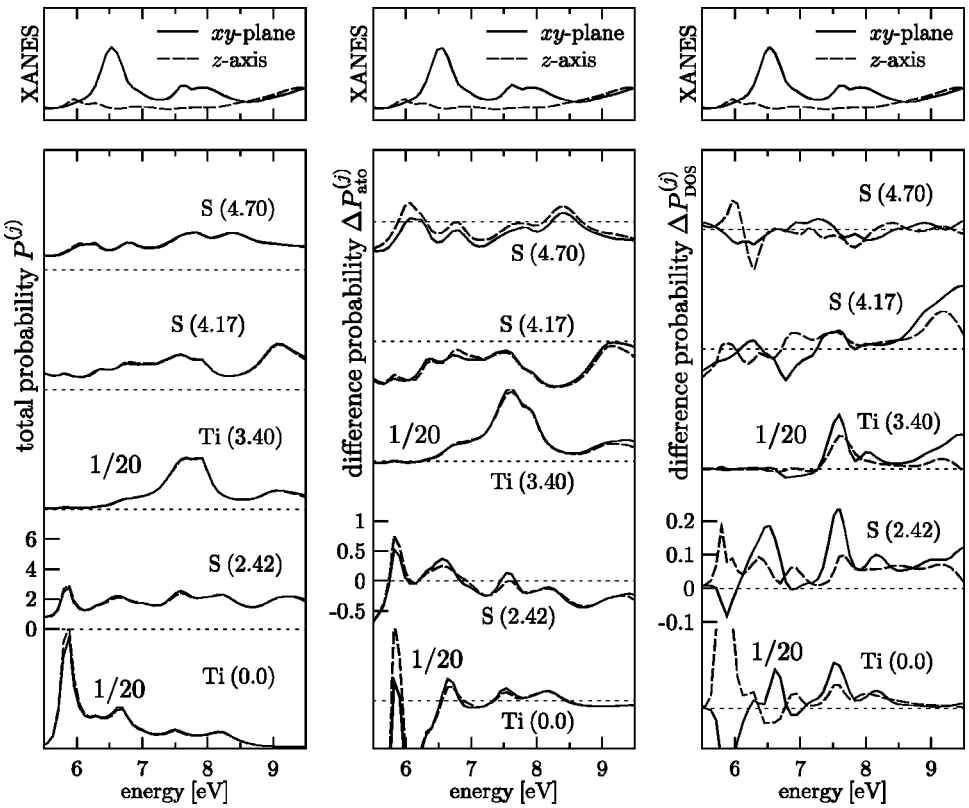

FIG. 1. Theoretical pre-peak structure of polarized Ti *K*-edge XANES of TiS_2 (upper panels), together with the photoelectron probability density $P^{(j)}$ (lower left panel), atomic difference probability density $\Delta P^{(j)}_{\rm ato}$ (lower middle panel), and DOS difference probability density $\Delta P^{(j)}_{\rm DOS}$ (lower right panel) around selected atoms. Solid lines correspond to the $\boldsymbol{\varepsilon}\|xy$ polarization, dashed lines to the $\boldsymbol{\varepsilon}\|z$ polarization. PEPD curves are identified by the chemical type of the appropriate atom and by its distance in Å from the center of the 135-atom cluster. Thin dotted lines mark zeros of $P^{(j)}$, $\Delta P^{(j)}_{\rm ato}$, and $\Delta P^{(j)}_{\rm DOS}$ for each subgraph. The absolute scale of the PEPD's is indicated at the lower panels; the scale of XANES is arbitrary. Note that curves for Ti atoms were divided by 20, as indicated.

The fine structure in PEPD differs from the XAFS. One might be surprised at first by the fact that this is the case not only for noncentral atoms but also for the photoabsorbing one (after all, XAS is approximately proportional to unoccupied DOS angularly projected on the central atom). One has to recall, however, that PEPD and XAS carry in fact different kind of information: While the XANES intensity informs us about the probability that the ejected electron goes anywhere, PEPD tells us how this ''anywhere'' looks like. Only a tiny fraction of the photoelectron density matrix (5), namely, that part of it which overlaps with the core of the central atom and which has the angular momentum character conforming to the dipole and/or quadrupole selection rules, enters indirectly into expressions for the XANES intensity, Eqs. (A6) and (A7).

One can see immediately from the lower left panel of Fig. 1 that the chemical type governs the gross shape of $P^{(j)}$ curves (we checked that this is true also for more distant atoms, which are not displayed here). The differences between PEPD's around atoms at crystallographically equivalent positions (say, Ti or S atoms belonging to different coordination spheres) comes first of all from the fact that this quantity is specifically related to the position of photoabsorbing atom, i.e., the site from which the photoelectron was ejected. (Apart from that, our finite-cluster approach obviously introduces inequality among otherwise equivalent sites.)

Hardly any polarization effect can be noticed in the $P^{(j)}$ or $\Delta P^{(j)}_{\rm ato}$ curves, despite the fact that the $\boldsymbol{\varepsilon}$ dependence in the XANES spectrum is quite significant. Only the difference probability $\Delta P^{(j)}_{\rm DOS}$, which emphasizes the effect of the particular site from which the photoelectron is ejected, displays a strong polarization dependence. This is a manifestation of the dominance of the DOS-generated unidirectional $P^{(j)}_{\rm DOS}$ contribution to the total PEPD, as mentioned in the end of Sec. II C.

Neither the local DOS nor $P_{\rm DOS}$ take into account that the photoelectron is *ejected from a particular site* via a dipole transition[20]—they are concerned with all electrons of a given energy equally. On the other hand, the probability $P^{(j)}$ that a Ti *K*-edge XAS photoelectron will be found near atom *j* differs, albeit slightly, from the probability of finding there ''any'' electron of the same energy. It is this small difference which reflects the fact that the TiS_2 crystal does not look identical when viewed from the Ti site either in the *xy*-plane or *z*-axis directions. So one has to resort to the difference probability $\Delta P^{(j)}_{\rm DOS}$ if the polarization-related features of PEPD are to be studied.

On the other hand, simple subtraction of the single-atom probability density $P^{(j)}_{\rm ato}$ does not provide a new insight. Due to the smoothness of atomic probability density $P^{(j)}_{\rm ato}$, the $P^{(j)}$ and $\Delta P^{(j)}_{\rm ato}$ curves look very similar, as can be seen in the left and middle panels of Fig. 1. The total probability density $P^{(j)}$ and atomic difference probability density $\Delta P^{(j)}_{\rm ato}$ carry essentially identical pieces of information.

As it follows from Fig. 1, there seems to be no simple correspondence between XANES peaks and peaks in the photoelectron probability density. Although for some atoms and/or peaks one can establish a visual connection between XANES and PEPD, for other features such a discernible connection is clearly absent. This lack of simple correspondence between XANES and PEPD peaks may be a manifestation of the interference nature of XAFS—it is generated not just

through accumulating electrons here and there but rather by interference between many scattering paths.

We performed also an angular momentum analysis of PEPD, according to Eqs. (23) and (24). We found that the *d* component dominates at Ti atoms (it contributes by more that 95% to either $P^{(j)}$ or $\Delta P^{(j)}_{\rm ato}$ or $\Delta P^{(j)}_{\rm DOS}$) and that the *p* component prevails at S atoms (comprises 60%–70% of PEPD). Moreover, practically all of the fine structure in PEPD is formed by the dominant *l* component (i.e., *d* at Ti and *p* at S atoms). This might again look surprising for someone who is accustomed to the conventional slang that the excited photoelectron has a *p* character at the *K*-edge due to the dipole selection rule. The point is that this would apply literally only in case that the final photoelectron state were an eigenstate of the angular momentum. On the other hand, the wave function $|\psi^{(-)}_{\boldsymbol{k}}\rangle$, which describes the exited photoelectron (as argued in Sec. II A), is not an angular momentum eigenstate. Rather, it is a superposition of states with different angular momenta, and the component with $l=2$ dominates at the central Ti site as a whole, while the relatively tiny component with $l=1$ determines the XANES intensity.

As mentioned, Wu *et al.*[27] suggest that the second-shell Ti atoms play a crucial role in generating the $\boldsymbol{\varepsilon}\|xy$ pre-peak. They arrived at this conclusion by observing that this pre-peak disappears if those six Ti atoms are removed from the cluster. A closer look at Fig. 1 reveals that the DOS-inclusive probability $P^{(j)}$ is, indeed, much higher near Ti atoms than near S atoms. However, this effect is clearly DOS related, having little connection with the particular direction of the photoelectron trajectory. By inspecting the DOS-corrected difference probability density $\Delta P^{(j)}_{\rm DOS}$ corresponding to the dominant pre-edge peak at $E=6.5$ eV, we can see that the largest effects *purely connected with x-ray absorption* actually occur at the nearest sulphur atoms. It is thus clear that nearest sulphur atoms definitely have their role in generating the $\boldsymbol{\varepsilon}\|xy$ pre-peak. In fact, we found that omitting six nearest S atoms from a large 135-atom cluster changes the calculated XANES drastically (making the very concept of pre-edge region inapplicable). Only the secondary-in-importance pre-edge peak at $E\approx 7.5$–8.0 eV seems to be generated by scattering off second-shell Ti atoms, as follows from the $\Delta P^{(j)}_{\rm DOS}$ curves in Fig. 1. It seems, therefore, that the physical picture of the process which is responsible for the $\boldsymbol{\varepsilon}\|xy$ pre-peak should consider the nearest sulphur atoms into account. Namely, although the total amount of the photoelectron density $P^{(j)}$ is small on sulphur atoms as compared with titaniums, its relatively modest variations with energy and polarization have a big impact on the XANES.

Let us emphasize that, strictly speaking, this kind of analysis only informs about sensitivity of the photoelectron density near individual atoms to the changes of polarization vector direction. It does not testify about the physical mechanism which may stand behind the creation of the pre-peak electron states. So our conclusions do not in fact contradict the suggestions that those states arise due to hybridization of central Ti $4p$ and next-neighboring Ti $3d$ orbitals[27] — both views may be rather complementary than opposing.

Finally, let us note that the new look on the role of nearest sulphurs we take here may be relevant to other non-centrosymmetric systems with a distinct XANES pre-peak, such as a colossal magnetoresistence material $La_{1-x}Ca_xMnO_3$ (Ref. 29).

B. Ti *K*-edge XANES of rutile TiO_2

The Ti *K*-edge XANES of rutile TiO_2 was studied very intensively due to its interesting pre-edge structure and the debate still continues.[6,30–33] In this paper, however, we want to concentrate on the extended XANES up to ~120 eV, as a comprehensive study of the effect of individual atoms on spectral peaks in this region was performed.[34,35] In rutile TiO_2, the Ti atoms are located at the center of a distorted octahedron. The plane containing four equatorial oxygens $O_{\rm eq}$ is parallel to the crystallographic *c* axis while two axial oxygens $O_{\rm ax}$ lie inside the plane defined by axes *a* and *b*. The third coordination sphere is formed by two titanium atoms $Ti_{\pm c}$, shifted from the central Ti by $\pm\boldsymbol{c}$. Instructive depictions of rutile TiO_2 structure can be found, e.g., in Fig. 3 of Ref. 32, Fig. 2 of Ref. 35, or Fig. 3 of Ref. 36.

Jeanne-Rose and Poumellec[35] studied how the polarized Ti *K*-edge XANES of TiO_2, calculated for a cluster of 25 atoms, is affected by variations in the positions of $O_{\rm ax}$ and $O_{\rm eq}$ atoms. That makes it possible for us to explore here to what extent does sensitivity of a spectral peak to a position of a certain atom imply high PEPD around that atom and *vice versa*. In accordance with the discussion in Sec. III A, we will concentrate more on the difference probability $\Delta P^{(j)}_{\rm DOS}$ than on $P^{(j)}$ itself.

In Fig. 2, theoretical polarized Ti *K*-edge XANES of TiO_2 is shown together with corresponding $P^{(j)}$, $\Delta P^{(j)}_{\rm ato}$, and $\Delta P^{(j)}_{\rm DOS}$ curves for the central Ti and its nearest neighbors. In order to connect with Jeanne-Rose and Poumellec,[35] we consider a cluster of 25 atoms. The notation of spectral peaks *C*, *D*, E_1, E_2, and E_3 is taken from Ref. 35, too. The *ad hoc* Fermi energy would be around 10 eV in the energy scale of Fig. 2, meaning that the wild oscillations at the beginning of the PEPD curves actually fall predominantly into the region of occupied states.

Let us now compare the conclusions of Jeanne-Rose and Poumellec[35] with the picture offered by the PEPD analysis. The equatorial oxygen $O_{\rm eq}$ was found to influence both the *C* and *D* peaks for both polarizations, the effect being significantly stronger on *D* than on *C* and for the $\boldsymbol{\varepsilon}\|c$ polarization than for the $\boldsymbol{\varepsilon}\|a$ polarization.[35] A counterpart to this effect can be found in the PEPD: A distinct peak in $\Delta P^{(j)}_{\rm DOS}$ around $O_{\rm eq}$ can be found at *D* and a mild feature at *C* for both polarizations; the *D* peak in $\Delta P^{(j)}_{\rm DOS}$ is higher for the $\boldsymbol{\varepsilon}\|c$ than for the $\boldsymbol{\varepsilon}\|a$ polarization.

When the position of the axial oxygen $O_{\rm ax}$ varies, the calculated $\boldsymbol{\varepsilon}\|a$ XANES is drastically altered at the *D* peak and not so much at the *C* peak, while the $\boldsymbol{\varepsilon}\|c$ spectrum is changed at the *C* peak only.[35] A brief look at the $O_{\rm ax}$ curves in Fig. 2 reveals that the largest $\Delta P^{(j)}_{\rm DOS}$ around the $O_{\rm ax}$ atom is at the *D* peak for the $\boldsymbol{\varepsilon}\|a$ spectrum and at the *C* peak for the $\boldsymbol{\varepsilon}\|c$ case. So, indeed, the energy at which a particular atom affects the photoelectron probability density most

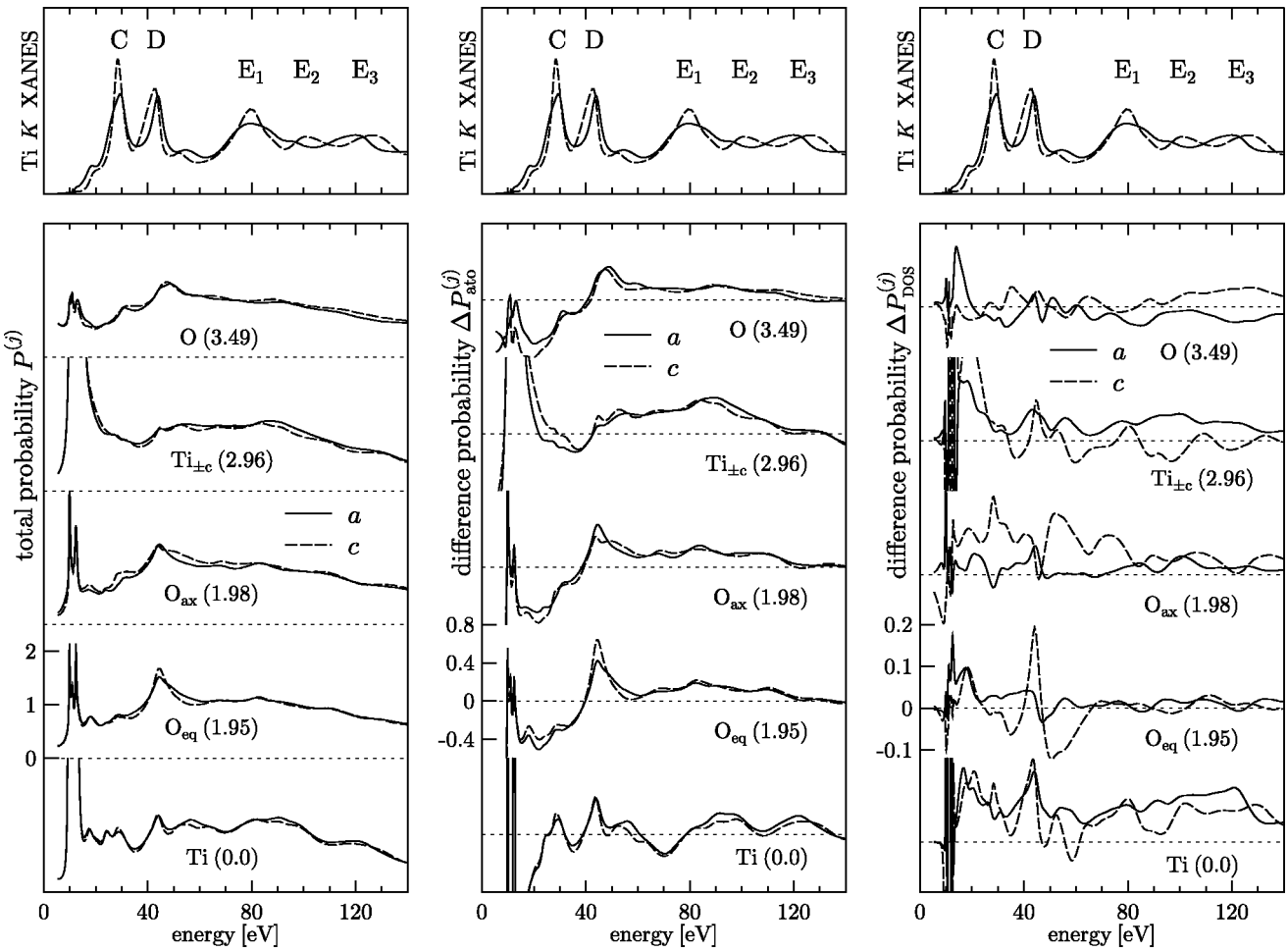

FIG. 2. Theoretical polarized Ti *K*-edge XANES of TiO_2 and corresponding PEPD curves. The meaning of the curves and symbols is analogous to that in Fig. 1.

prominently coincides in this case with the energy at which the XANES is significantly changed when that atom is moved. The analogy is nevertheless only a qualitative one—larger $\Delta P^{(j)}_{\mathrm{DOS}}$ does not necessarily imply bigger changes of XANES peaks when O_{ax} is moved. For example, the *C* resonance in $\Delta P^{(j)}_{\mathrm{DOS}}$ for $\boldsymbol{\varepsilon}\|c$ is stronger than the *D* resonance for $\boldsymbol{\varepsilon}\|a$, and yet the exact position of the O_{ax} atom affects more the *D* spectral peak at $\boldsymbol{\varepsilon}\|c$ than the *C* peak at $\boldsymbol{\varepsilon}\|a$ polarization.[35] On the other hand, the total probability density $P^{(j)}$ is larger at the *D* peak energy than at the *C* peak for both oxygens, reflecting correctly the greater sensitivity of the *D* peak to their positions.

So the following intuitively plausible picture emerges: For comparing XANES peaks at different energies, the total probability $P^{(j)}$ may be a good indication of their respective sensitivity to atomic positions. For investigating polarization effects, one has to resort to $\Delta P^{(j)}_{\mathrm{DOS}}$.

Unlike for the *C* and *D* peaks, a correspondence between XANES and $\Delta P^{(j)}_{\mathrm{DOS}}$ peaks cannot be established for the E_i maxima. Jeanne-Rose and Poumellec[35] found that the E_2 peak in the $\boldsymbol{\varepsilon}\|c$ spectrum is affected quite a lot by the O_{eq} movement while peaks E_1 and E_3 are left basically intact for either polarization—a property that does not seem to have a counterpart in Fig. 2. The sensibility of a XANES peak to a movement of a particular atom, hence, does not necessarily imply a high localization of the photoelectron around that atom—which can be found only by a proper PEPD calculation.

It is worth noting that if single-scattering dominates in generating a particular XANES peak (such as *C* for the $\boldsymbol{\varepsilon}\|a$ polarization),[35] one can observe a distinct resonance in $\Delta P^{(j)}_{\mathrm{DOS}}$ at corresponding energy. On the other hand, such a correspondence appears to be blurred for spectral peaks where a significant contribution from multiple-scattering is suspected (such as the *C* peak at the O_{ax} atom for the $\boldsymbol{\varepsilon}\|a$ polarization or the E_2 peak at O_{eq} and $Ti_{\pm c}$for the $\boldsymbol{\varepsilon}\|c$ polarization).[35] This seems to be plausible—a multiple-scattering nature of a peak emphasizes that it is generated not by a mere ''presence'' of the photoelectron near certain atom but rather by a complicated interference process. It remains to be explored to what extent this trend is a general one.

IV. DISCUSSION

The photoelectron probability density offers us a direct look on the spatial localization of those electron states which are seen by XAS. Contrary to a bit vague concepts like importance of various atoms for the formation of a particular

XANES peak or order of multiple scattering which has to be accounted for, PEPD is a rigorously defined quantity with a transparent physical interpretation. Hence even if there were no immediate practical applications, PEPD analysis would still remain a valuable tool for understanding the physical processes which give rise to the XANES spectrum. Apart from this principal asset, there are two directions where PEPD analysis could contribute to solving concrete problems: investigations of real structure of solids and investigations of their electronic structure.

One of the obstacles to overcome when fitting the experimental XANES spectrum with calculated spectra of trial structures is that one has, in general, a lot of atoms to move and hence it is difficult to identify those whose positions are most critical for the XANES shape. By providing a deeper insight into the ''photoelectron trajectory,'' PEPD analysis may drop a hint for the most critical spots in advance. Intuitive arguments and practical experience (Sec. III) show that both $P^{(j)}$ and $\Delta P^{(j)}_{\mathrm{DOS}}$ reflect the sensitivity of XANES to movement of individual atoms: The total probability density $P^{(j)}$ is more relevant for comparing the roles of different chemical species while $\Delta P^{(j)}_{\mathrm{DOS}}$ is more indicative of the polarization and site dependence of XANES spectra.

In electronic structure studies, the appealing feature of PEPD is that it directly investigates those unoccupied states which are probed by XAS. When investigating the spatial localization of these states, one is thus not left relying on heuristic arguments like ''which atom affects the spectrum most if moved.'' One can even explore the angular momentum character of XANES states by projecting the wave functions $\psi^{(-)}_{\boldsymbol{k}}$ along Eqs. (23) and (24). In that way, one can see not only from which atom a particular XANES peak arises but also from what type of orbital is comes from.

The concept of PEPD relates, of course, not just to the XANES region but to the EXAFS part of the absorption spectrum as well. The reason why we mention only XANES here explicitly is that EXAFS oscillations can be properly analyzed with other tools. Note also that the PEPD analysis could be applied to photoelectron diffraction as well — one would just have to omit the angular integration $\int d^2\hat{\boldsymbol{k}}$ in Eqs. (7) and (22) and in related expressions.

V. CONCLUSIONS

Our analysis demonstrates that it makes sense to explore the probability that a photoelectron participating in a XANES process can be found at a specific place. The relevant quantity is the photoelectron probability density and it can be calculated as a sum of squares of wave functions describing elementary PED processes, weighted by normalized PED cross sections. When investigated as a function of the photoelectron energy, it exhibits a resonancelike structure and depends on the atom around which it is evaluated. The bulk of PEPD is dominanted by DOS-like effects, meaning that, e.g., hardly any polarization dependence can be seen in it unless the DOS-related portion is subtracted. In many cases, the high difference probability $\Delta P^{(j)}_{\mathrm{DOS}}$ around an atom may serve as an indication of the high sensitivity of XANES towards the position of that atom for a given energy. The fine structure in PEPD does not copy the corresponding XANES: For some atoms and/or peaks, a visual connection between XANES and PEPD can be established; for other features such a discernible connection is absent. This may be a manifestation of the interference nature of XAFS — the correspondence between XAS and PEPD peaks is more often observed for features which arise from single scattering than for multiple-scattering peaks. The spatial dependence of PEPD thus provides information which is not equivalent to what can be learned from comparing theoretical spectra for various trial structures but rather is complementary to it.

By performing a PEPD analysis for a Ti *K*-edge of TiS_2, we found that, contrary to earlier interpretations, the sulphur atom nearest to the absorbing titanium participates significantly in formation of the distinct polarization dependence of the pre-peak.

ACKNOWLEDGMENTS

This work was supported by Grant No. 202/99/0404 of the Grant Agency of the Czech Republic. The use of the CRYSTIN structural database was financed by Grant No. 203/99/0067 of the Grant Agency of the Czech Republic. The author is grateful to A. Šimůnek for stimulating discussions and for a critical reading of the manuscript.

APPENDIX A: OTHER EXPRESSIONS FOR PED AND XAS CROSS SECTIONS

In this appendix, some other formulations of the equations presented in Sec. II B are shown, in order to facilitate connection with notations and definitions in other works.

The photoelectron diffraction cross section, evaluated in Eq. (18), can be expressed as

$$\frac{d\sigma}{d\Omega_{\boldsymbol{k}}}=\frac{1}{4\pi}\alpha\omega k\left[\left|\sum_L \beta^{(0)}_L(\boldsymbol{k})D^*_{LL_c}\right|^2 + \frac{1}{16}\alpha^2\omega^2\left|\sum_L \beta^{(0)}_L(\boldsymbol{k})Q^*_{LL_c}\right|^2\right]. \tag{A1}$$

By introducing the scattering matrix W of Eq. (14) directly into Eq. (18), one obtains

$$\frac{d\sigma}{d\Omega_{\boldsymbol{k}}}=4\pi\alpha\omega k\left[\left|\sum_L \sum_{jL''} W^{0j}_{LL''} i^{l''} Y^*_{L''}(\hat{\boldsymbol{k}}) e^{i\boldsymbol{k}(\boldsymbol{R}^j-\boldsymbol{R}^0)} D^*_{LL_c}\right|^2 + \frac{1}{16}\alpha^2\omega^2\left|\sum_L \sum_{jL''} W^{0j}_{LL''} i^{l''} Y^*_{L''}(\hat{\boldsymbol{k}}) e^{i\boldsymbol{k}(\boldsymbol{R}^j-\boldsymbol{R}^0)} Q^*_{LL_c}\right|^2\right], \tag{A2}$$

which is analogous to Eq. (22a) of Natoli *et al.*[18]

As a lot of useful relations about XAS and PED within the *wave function formalism* can be found in Ref. 16, we quote here the relation between the ''outgoing'' quantities used in that paper and the ''incoming'' quantities employed here. The scattering amplitude $\beta^{(j)}_L(L'')$ of Eq. (13) is connected with the amplitude $B^{(j)}_L(L'')$ of Eq. (2.28) of Natoli *et al.*[16] via

$$\beta_L^{(j)}(L'') = (-1)^m [B^{(j)}_{l,-m}(l'',-m'')]^* (-1)^{m''}, \quad \text{(A3)}$$

and the scattering matrix W relates to the matrix

$$Z^{ij}_{LL'} \equiv [(\underline{T}+\underline{H})^{-1}]^{ij}_{LL'}$$

of Eq. (3.3) of Natoli *et al.*[16] as

$$W^{ij}_{LL'} = (-1)^m [Z^{ij}_{(l,-m)(l',-m')}]^* (-1)^{m'} \quad \text{(A4)}$$

and to the τ matrix of Refs. 37 and 38 as

$$W^{ij}_{LL'} = -(-1)^{m'} [\tau^{ji}_{(l',-m')(l,-m)}]^* (-1)^m. \quad \text{(A5)}$$

Employing the Z and τ matrices, the x-ray absorption cross section of Eq. (21) can be written as

$$\sigma_{\mathrm{XAS}} = 4\pi\alpha\omega k \sum_{LL'} \left\{ \mathrm{Im}(D^*_{LL_c} Z^{00}_{LL'} D_{L'L_c}) + \frac{1}{16}\alpha^2\omega^2 \mathrm{Im}(Q^*_{LL_c} Z^{00}_{LL'} Q_{L'L_c}) \right\} \quad \text{(A6)}$$

or as

$$\sigma_{\mathrm{XAS}} = -4\pi\alpha\omega k \sum_{LL'} \left\{ \mathrm{Im}(D_{LL_c} \tau^{00}_{LL'} D^*_{L'L_c}) + \frac{1}{16}\alpha^2\omega^2 \mathrm{Im}(Q_{LL_c} \tau^{00}_{LL'} Q^*_{L'L_c}) \right\}. \quad \text{(A7)}$$

Equations (A6) and (A7) can be arrived at either by invoking the Green function formalism from the beginning or by applying the optical theorem to Eq. (21), as outlined by Natoli *et al.*[16]

APPENDIX B: PEPD IN CASE OF A SINGLE ATOM

In calculating the single-atom probability density $P_{\mathrm{ato}}(\boldsymbol{r})$, one can proceed just as in Sec. II B. The only difficulty arises in expanding the solution of a single-atom Lippman-Schwinger equation inside (now) empty spheres around sites $\boldsymbol{R}^j$. One cannot mechanically employ Eqs. (12)–(14) to find the amplitudes $\beta_L^{(j)}(\boldsymbol{k})$, as the phase shifts at noncentral atomic sites are zero now. Instead, by applying formula for reexpanding $j_l(k|\boldsymbol{R}^p|)Y_L(\boldsymbol{R}^p)$ and $n_l(k|\boldsymbol{R}^p|)Y_L(\boldsymbol{R}^p)$around different origins, one can arrive at the following expression for $\beta_L^{(j)}(L'')$:

$$\beta_L^{(j)}(L'') = e^{-i\delta^{(0)}_{l''}} 4\pi \sum_{pL'} i^{l-l''+l'} [j_{l'}(k|\boldsymbol{R}^p|)\cos\delta^{(0)}_{l''} - n_{l'}(k|\boldsymbol{R}^p|)\sin\delta^{(0)}_{l''}] Y_{L'}(\boldsymbol{R}^p) C^{L''}_{LL'}, \quad \text{(B1)}$$

which ought to be inserted into Eq. (22) with the help of Eq. (12), together with replacement of the single-center radial wave function $\mathcal{R}_l^{(j)}(kr)$ with its free-electron counterpart $j_l(kr)$.

APPENDIX C: TECHNICAL DETAILS OF PEPD CALCULATIONS

When evaluating the PEPD defined by Eqs. (22) and (25), we rely on the expression

$$P^{(j)} = \frac{16\pi^2}{\sigma_{\mathrm{XAS}}} \int d^2\hat{\boldsymbol{k}} \frac{d\sigma}{d\Omega_{\boldsymbol{k}}} \sum_L \left| \sum_{L''} i^{l''} \beta_L^{(j)}(L'') Y^*_{L''}(\hat{\boldsymbol{k}}) \right|^2 \times \int_0^{R_N^{(j)}} dr r^2 [R_l^{(j)}(kr)]^2, \quad \text{(C1)}$$

where the photoelectron diffraction cross section is evaluated from Eq. (18) and the amplitudes $\beta_L^{(j)}(L'')$ from Eq. (13). The angular $\hat{\boldsymbol{k}}$ integration in Eq. (C1) could be performed analytically in principle. However, that would lead to such a proliferation of slowly convergent sums over angular momenta that it is actually computationally more convenient to keep the $\hat{\boldsymbol{k}}$ integral in the expression (C1) and to evaluate it numerically.

The angular momentum sum Σ_L in Eq. (C1) descends from Eq. (10) and converges quite quickly (it corresponds to a multicenter expansion in the terminology of Durham *et al.*).[37] In all the cases analyzed in Sec. III, it was sufficient to cut this sum at $l_{\max}=3$. On the other hand, the sum $\Sigma_{L''}$, which descends into Eq. (C1) from the expansion (13), corresponds to a single-center expansion and converges only slowly. In this work it was cut at $l_{\mathrm{inc}}=30$, which we found to be a safe value. Taking $l_{\mathrm{inc}}=20$ would still lead to an acceptable accuracy, while increasing l_{inc} up to 40 did not induce significant changes with respect to the $l_{\mathrm{inc}}=30$ case.

The angular integration was performed in two ''perpendicular'' spherical coordinates θ, ϕ as

$$\int d^2\hat{\boldsymbol{k}} \rightarrow \int_0^{\pi} d\theta \sin\theta \int_0^{2\pi} d\phi. \quad \text{(C2)}$$

In Sec. III, 50 points were used for numerical integration over the θ coordinate and $2\times 50\times \sin\theta$ points for integration over ϕ. We checked that such a grid is dense enough to guarantee a sufficient accuracy.

[1] D.D. Vvedensky, J.B. Pendry, U. Döbler, and K. Baberschke, Phys. Rev. B **35**, 7756 (1987).
[2] X.S. Feng and J.C. Tang, Surf. Sci. **314**, 365 (1994).
[3] L.A. Bugaev, Ph. Ildefonse, A.M. Flanks, A.P. Sokolenko, and H.V. Dmitrienko, J. Phys.: Condens. Matter **12**, 1119 (2000).
[4] S. Della Longa, A. Arcovito, M. Girasole, J.L. Hazemann, and M. Benfatto, Phys. Rev. Lett. **87**, 155 501 (2001).
[5] O. Šipr, A. Šimůnek, S. Bocharov, Th. Kirchner, and G. Dräger,

Phys. Rev. B **60**, 14 115 (1999).
[6] F. Farges, G.E. Brown, and J.J. Rehr, Phys. Rev. B **56**, 1809 (1997).
[7] S.I. Zabinsky, J.J. Rehr, A. Ankudinov, R.C. Albers, and M.J. Eller, Phys. Rev. B **52**, 2995 (1995).
[8] Yu.F. Migal, Phys. Status Solidi B **212**, 3 (1999).
[9] J.E. Müller and J.W. Wilkins, Phys. Rev. B **29**, 4331 (1984).
[10] D. Dill and J.L. Dehmer, J. Chem. Phys. **61**, 692 (1974).
[11] P.A. Lee, Phys. Rev. B **13**, 5261 (1976).
[12] D.D. Vvedensky, in *Unoccupied Electronic States*, edited by J.C. Fuggle and J.E. Inglesfield (Springer, Berlin, 1992), p. 139.
[13] O. Šipr, J. Synchrotron Radiat. **8**, 232 (2001).
[14] J. Mustre de Leon, J.J. Rehr, C.R. Natoli, C.S. Fadley, and J. Osterwalder, Phys. Rev. B **39**, 5632 (1989).
[15] H.A. Bethe and E.E. Salpeter, *Quantum Mechanics of One- and Two-Electron Atoms* (Springer, Berlin, 1957), p. 295.
[16] C.R. Natoli, M. Benfatto, and S. Doniach, Phys. Rev. A **34**, 4682 (1986).
[17] H.A. Bethe, Ann. Phys. (Leipzig) **4**, 443 (1930); G. Breit and H.A. Bethe, Phys. Rev. **93**, 888 (1954).
[18] C.R. Natoli, M. Benfatto, C. Brouder, M.F. Ruiz López, and D.L. Foulis, Phys. Rev. B **42**, 1944 (1990).
[19] J.J. Rehr, C.H. Booth, F. Bridges, and S.I. Zabinsky, Phys. Rev. B **49**, 12 347 (1994).
[20] O. Šipr, J. Phys.: Condens. Matter **13**, 8519 (2001).
[21] See, e.g., W.E. Pickett, Comput. Phys. Rep. **9**, 115 (1989).
[22] W. Kohn and L.J. Sham, Phys. Rev. **140**, A1133 (1965).
[23] G. Bergerhoff, R. Hundt, R. Sievers, and I.D. Brown, J. Chem. Inf. Comput. Sci. **23**, 66 (1983).
[24] S. Bocharov, G. Dräger, D. Heumann, A. Šimůnek, and O. Šipr, Phys. Rev. B **58**, 7668 (1998).
[25] O. Šipr, P. Machek, A. Šimůnek, J. Vackář, and J. Horák, Phys. Rev. B **56**, 13 151 (1997).
[26] F. Al Shamma, M. Abbate, and J.C. Fuggle, in *Unoccupied Electron States*, edited by J.C. Fuggle and J.E. Inglesfield (Springer, Berlin, 1992), p. 347.
[27] Z.Y. Wu, G. Ouvrard, P. Moreau, and C.R. Natoli, Phys. Rev. B **55**, 9508 (1997).
[28] A. Šimůnek, O. Šipr, S. Bocharov, D. Heumann, and G. Dräger, Phys. Rev. B **56**, 12 232 (1998).
[29] F. Bridges, C.H. Booth, G.H. Kwei, J.J. Neumeier, and G.A. Sawatzky, Phys. Rev. B **61**, R9237 (2000).
[30] C. Brouder, J.-P. Kappler, and E. Beaurepaire, in *Proceedings of the 2nd European Conference on Progress in X-ray Synchrotron Radiation Research, Roma, 1990*, edited by A. Balerna, E. Bernieri, and S. Mobilio (SIF, Bologna, 1990), p. 19.
[31] T. Uozumi, K. Okada, A. Kotani, O. Durmeyer, J.P. Kappler, E. Beaurepaire, and J.C. Parlebas, Europhys. Lett. **18**, 85 (1992).
[32] Z.Y. Wu, G. Ouvrard, P. Gressier, and C.R. Natoli, Phys. Rev. B **55**, 10 382 (1997).
[33] Y. Joly, D. Cabaret, H. Renevier, and C.R. Natoli, Phys. Rev. Lett. **82**, 2398 (1999).
[34] V. Jeanne-Rose, B. Poumellec, and Y. Aïfa, J. Phys. IV **7**, C2-221 (1997).
[35] V. Jeanne-Rose and B. Poumellec, J. Phys.: Condens. Matter **11**, 1123 (1999).
[36] B. Poumellec, R. Cortes, G. Tourillon, and J. Berthon, Phys. Status Solidi B **164**, 319 (1991).
[37] P.J. Durham, J.P. Pendry, and C.H. Hodges, Comput. Phys. Commun. **25**, 193 (1982).
[38] D.D. Vvedensky, D.K. Saldin, and J.B. Pendry, Comput. Phys. Commun. **40**, 421 (1986).